Low-noise short-wavelength pumped frequency downconversion for quantum frequency converters

Geus, Jan Fabian ; Elsen, Florian ; Nyga, Sebastian ; Stolk, A.J.; van der Enden, K.L.; van Zwet, E.J.; Haefner, Constantin ; Hanson, R.; Jungbluth, Bernd

Citation (APA)
Geus, J. F., Elsen, F., Nyga, S., Stolk, A. J., van der Enden, K. L., van Zwet, E. J., Haefner, C., Hanson, R., & Jungbluth, B. (2024). Low-noise short-wavelength pumped frequency downconversion for quantum frequency converters. *Optica Quantum*, *2*(3), 189-195. https://doi.org/10.1364/OPTICAQ.515769

Important note
To cite this publication, please use the final published version (if applicable).
Please check the document version above.

OPTICA QUANTUM

Low-noise short-wavelength pumped frequency downconversion for quantum frequency converters

Jan Fabian Geus,[1,2,*] **Florian Elsen,**[1,2] **Sebastian Nyga,**[1] **Arian J. Stolk,**[3,4] **Kian L. van der Enden,**[3,4] **Erwin J. van Zwet,**[3,5] **Constantin Haefner,**[1,2] **Ronald Hanson,**[3,4] **and Bernd Jungbluth**[1]

[1] *Fraunhofer Institute for Laser Technology ILT, Steinbachstr. 15, D-52074 Aachen, Germany*
[2] *RWTH Aachen University LLT - Chair for Laser Technology, Steinbachstr. 15, D-52074 Aachen, Germany*
[3] *QuTech Delft University of Technology, 2628 CJ Delft, The Netherlands*
[4] *Kavli Institute for Nanoscience, Delft University of Technology, 2628 CJ Delft, The Netherlands*
[5] *Netherlands Organisation for Applied Scientific Research (TNO), P.O. Box 155, 2600 AD Delft, The Netherlands*
*jan.fabian.geus@ilt.fraunhofer.de

We present a highly efficient low-noise quantum frequency converter from the visible range to telecom wavelengths, combining a pump laser at intermediate frequency resonantly enhanced in an actively stabilized cavity with a monocrystalline bulk crystal. A demonstrator for photons emitted by nitrogen-vacancy-center qubits achieves 43% external efficiency with a noise photon rate per wavelength (frequency) band of 2 s^{-1}/pm(17 s^{-1}/GHz) – reducing the noise by two orders of magnitude compared with current devices based on periodically poled crystals with waveguides. With its tunable output wavelength, this device enables the generation of indistinguishable telecom photons from different network nodes and is, as such, a crucial component for a future quantum internet based on optical fiber.

1. INTRODUCTION

A future quantum internet (QI) [1,2], where quantum processor nodes are connected via optical channels, holds the promise for applications such as secure communication, distributed quantum computation, and enhanced sensing [3–5]. Previously, the generation of entanglement between separated processing nodes has been realized with ions and atoms [6–9], quantum dots [10,11] and nitrogen-vacancy (NV) centers in diamond [12,13]. Additionally, other platforms such as rare-earth-doped crystals [14–16], mechanical resonators [17], and atom-cloud-based memories [18,19] have been used to explore the distribution of entangled states toward functioning as quantum transducer or repeater in quantum networks.

Essential to commonly used remote entanglement generation protocols [7–13] is interfering single photons that are entangled with stationary qubits in the nodes, mediated by propagation over fiber. For such protocols to operate at long distance, photon loss in fibers is a dominant factor determining the entanglement generation rate. Leading platforms for realizing processor nodes [8,20–24] have natural emission wavelengths in the visible spectrum; fiber losses at these wavelengths prevent useful scaling beyond a few kilometers. However, absorption in an optical fiber is at its global minimum in the vicinity of 1550 nm [25]. The wavelength of the emitted photons from the processing nodes can be converted to the low-absorption region of an

optical fiber by frequency conversion, preserving the photons correlated or entangled with the qubit's state [26–29]. When linking separate QI network nodes, state-preserving frequency conversion of single photons is thus an important part of the quantum interface, enabling long-range transmission through optical fiber. This entanglement of the photons with a solid-state spin-qubit was recently demonstrated for NV centers [30], which is the main focus of this work.

In this work we propose a new approach to frequency conversion of photons emitted by qubits from the visible range to telecom wavelengths, which can enable as efficient conversion as state-of-the-art devices, but potentially induces only a negligible rate of uncorrelated information, i.e., noise photons. This approach is demonstrated for the frequency conversion from the fluorescence wavelength of NV-center qubits ($\lambda^{NV} = 637.24$ nm) to the telecom L-band with a strong pump laser at $\lambda_P = 1064$ nm. To achieve high rates of entanglement generation between separate nodes connected by an optical fiber, two important requirements to a device incorporating frequency conversion of photons (quantum frequency converter; QFC) must be fulfilled. First, photons emitted by the network node must be converted to the telecom wavelength range with a probability close to unity. Second, to guarantee high signal-to-noise ratios (SNRs), the QFC must not add noise photons to the transmission channel. A QFC for the downconversion of light at the

single-photon level is typically realized by three-wave mixing (TWM) [31–35] in a nonlinear material (NLM), usually a periodically poled crystal with a waveguiding structure, by mixing the single-photon input (wavelength λ_{in}) with a high-intensity field (λ_P) to generate single photons at the difference frequency (λ_{out}). Obeying the law of conservation of energy in this case ($\lambda_{in}^{-1} = \lambda_p^{-1} + \lambda_{out}^{-1}$), the following wavelength configurations can be distinguished:

$$\begin{aligned} \lambda_P < \lambda_{out} \text{ for } \lambda_{in} < \lambda_{out}/2 \text{ ("short - wavelength pumped")} \\ \lambda_P > \lambda_{out} \text{ for } \lambda_{in} > \lambda_{out}/2 \text{ ("long - wavelength pumped")} \end{aligned} \quad \textbf{(1)}$$

The internal conversion efficiency η_{int} of a QFC can in principle reach unity; values exceeding 70% [36] were previously demonstrated for a downconversion set-up from λ^{NV} to the telecom L-band. Here, η_{int} equals the rate of generated photons at λ_{out} behind the QFC divided by the rate of photons at λ_{in} incident to the QFC and corrected for all losses. Most significant losses are introduced by the required spectral filters and the free space to single-mode coupling when the fields enter the waveguide and subsequently a single-mode optical fiber for long-range transmission, limiting the total device efficiency (i.e., external efficiency) of demonstrated QFCs to below 60% [24,37].

In the following section, the processes leading to the generation of noise photons at the output wavelength are discussed, assuming narrow spectral filtering around λ_{out}. Noise photons are generated in a QFC due to the presence of high-intensity pump radiation in the NLM and result either from Raman scattering or spontaneous parametric downconversion (SPDC) of pump photons. Furthermore, noise photons are produced from black-body radiation. However, the latter process is negligible compared with SPDC or Raman scattering in state-of-the-art devices. When λ_P and λ_{out} are sufficiently far apart, Raman scattering is suppressed and will potentially not contribute to the generation of noise photons at λ_{out}, whereas SPDC creates photon pairs from the statistical decay of pump photons, which therefore are located on the long wavelength side of λ_P. Hence, for long-wavelength-pumped TWM, only anti-Stokes Raman scattering (or higher order processes) contributes to the generation of uncorrelated information [38], whereas for short-wavelength-pumped TWM, SPDC of pump photons can dominate the generation of noise at λ_{out}.

In state-of-the-art devices, periodically poled NLM with waveguiding structures are used. While efficient conversion with low pump power is possible due to the confinement of the interacting waves, random duty-cycle (RDC) errors in the spatial parameters of periodicity and waveguide result in elevated efficiency of the SPDC noise process which can be larger by orders of magnitude than for a birefringently phase-matched configuration [39,40]. This process was theoretically investigated in [41]. For a statistical deviation σ_l from the mean period length l, the rate of SPDC noise photons additionally generated by the existence of RDC errors, n_{SPDC}^{RDC}, is described by

$$n_{SPDC}^{RDC} = \frac{N_{pm}}{N_D} \left[1 - \exp\left(-\frac{\pi^2 \sigma_l^2}{2l^2} \right) \right], \quad \textbf{(2)}$$

where N_{pm} denotes the rate of converted photons in perfectly phase-matched conditions ($\Delta k = 0$) for the wavelength combination of the noise-generation process (1064 nm → 1589 nm + 3220 nm) and N_D equals the number of domains. This effect can be reduced by reducing the RDC errors of periodically poled materials. In a QFC incorporating a periodically poled

bulk crystal without waveguide confinement, a significant reduction by roughly a factor of five was achieved [36]. To further reduce this effect, the poling quality of NLM must be improved, which implies higher manufacturing costs. Even in the ideal case of zero RDC errors, the rate of SPDC-generated noise will remain non-zero due to the non-vanishing efficiency of off-phase-matched conversion.

To investigate the rate of SPDC-generated noise without the effect of RDC errors, one can use a monocrystalline NLM, i.e., implementing birefringent phase matching. With a variety of those materials being available at low cost, a significant reduction of noise photons may be available without excessive cost demand. In case of birefringent phase matching, the conversion efficiency of a three-wave mixing process in an NLM of length L at the low-gain limit (i.e., $\Gamma^2 \ll (\Delta k/2)^2$, see [42]) is proportional to

$$\mu_c \propto \text{sinc}^2\left(\Delta k \times \frac{L}{2} \right), \quad \textbf{(3)}$$

with the phase mismatch Δk ([43]) and the gain factor Γ, which satisfies ([42])

$$\Gamma^2 = \frac{2\omega_{in}\omega_{out}|d_{eff}|^2 I_p}{n_{in}n_{out}n_p\epsilon_0 c^3}, \quad \textbf{(4)}$$

where $\omega_{in/out}$ denote angular frequencies, I_p pump laser intensity, $n_{in/out/p}$ the indices of refraction, and d_{eff} the material's effective nonlinear coefficient. To confirm the applicability of Eq. (3) to the case of the SPDC-generated photons, one must calculate the gain factor and phase mismatch for the respective experimental conditions. In the case investigated here, high pump powers are present in the NLM, but the phase mismatch for the SPDC process is large. Hence, the low-gain approximation remains valid for this case. The explicit calculation is presented in section 3.1.

Therefore, if Raman noise can be neglected and the material parameters are chosen to result in a large phase mismatch and thus strongly suppressed efficiency of the SPDC process, the noise generated by quantum frequency converters may be reduced to negligible levels. Note that spectral filtering will always remain a requirement for low-noise conversion, since the amplitudes of both Raman scattering and SPDC strongly vary with the wavelength of the generated photons. While the applicability of the semi-classical approximation to the single-photon level is arguable, we assume that the average rate of SPDC-generated noise photons will be of similar orders of magnitude when quantum effects are considered. An alternative approach to circumvent high rates of noise is a two-step conversion scheme with an intermediate conversion to the near infrared [41], i.e., realizing a long-wavelength pumped QFC from the visible range, which adds losses and increases complexity.

In this work, we investigate a single-stage QFC scheme for the conversion of photons emitted by NV centers at $\lambda^{NV} = \lambda_{in} = 637.24$ nm to $\lambda_{out} = 1589$ nm, resulting in a short-wavelength pumped configuration ($\lambda_P = 1064$ nm). In current generation short-wavelength pumped periodically poled lithium niobate (ppLN)-based QFCs with waveguided interaction (ppLN waveguide QFC), the spectral density of noise photons (NSD) introduced to the transmission channel per time interval equals 250 s^{-1}/pm (2.1×10^3 s^{-1}/GHz) [31]. In a recent work, an improvement by a factor of five was demonstrated with a QFC based on a ppKTP crystal without a waveguide in a passive enhancement cavity (cavity-assisted ppKTP QFC), where an NSD of 45 s^{-1}/pm at an external conversion efficiency of 33 % was demonstrated [36], confirming that noise can be decreased

by making use of higher-quality periodically poled materials. However, further work must be conducted. For a strictest possible bandwidth of 50 MHz (limited by the bandwidth of the downconverted photons), the ppLN waveguide QFC (cavity-assisted ppKTP QFC) therefore adds error counts with a rate of approximately 100 s^{-1} (20 s^{-1}). Since dark-count rates of single-photon detectors can be below 10 s^{-1}, the QFC is the main source of noise events, and thus limits the achievable fidelity of entanglement generation. A previous experiment [44] involving two state-of-the-art NV-center nodes combined with waveguide-based ppLN QFCs highlight the need for low noise solutions. In this interference experiment, the average SNR after ultra-narrow spectral and time filtering was approximately 15, with the major noise contribution by the QFCs. Without any improvements in noise reduction, the usage of the single-click protocol for entanglement generation of two NV-center qubits [22,45] intrinsically reduces the signal brightness (i.e., the bright state population of the NV center) to limit the probability of double photon events at the central beam splitter between the two qubits, which may not result in an entangled state. At a modestly reduced signal brightness (10 %), this would result in a SNR of 1.5 (3 in the case of cavity-assisted ppKTP QFC), prohibiting entanglement generation.

In the following section, we demonstrate that a conversion scheme in birefringent phase-matching configuration enables highly efficient conversion with smaller noise counts than in any other configuration for the wavelength combination investigated here. The overall device efficiency is as high as in state-of-the-art QFCs, while reducing the number of noise counts by more than two orders of magnitude compared with a ppLN waveguide QFC and by a factor of 20 compared with a cavity-assisted ppKTP QFC.

2. CONCEPT

In state-of-the-art devices, periodically poled crystals with waveguiding structures are used because they enable high conversion efficiency with low-power pump lasers. At the same time, high rates of noise photons are introduced. We propose a TWM scheme without the use of a periodically poled material and waveguiding structures, i.e., TWM in a monocrystalline bulk material. This approach requires birefringent phase matching for efficient conversion, which requires orthogonal polarization of the interacting waves. For most NLM, the effective nonlinearity is smaller if the phase-matching condition is met in Type-I or Type-II configuration compared with the effective nonlinearity in Type-0 configuration in the case of quasi-phase matching in pp-NLM. To overcome this challenge, larger pump laser intensities are required, which can be achieved by resonantly enhancing the pump laser power in an optical cavity. Relying on active stabilization of the cavity, which can be accomplished with low-cost electronic components, enables maintaining efficient conversion while the pump wavelength is tuned, resulting in a tunable output wavelength. Since the central wavelength of photons emitted by NV-center qubits can drift by up to 10 MHz/min, a tunable QFC output wavelength is required to maintain indistinguishable telecom photons. Whereas similar set-ups have been proposed for QFC [36,46,47] and photon-pair generation [48], they incorporate periodically poled crystals and passively stabilized cavities to achieve the required efficiency.

In this letter, monocrystalline KTA is chosen as the NLM, exhibiting a broad transparency range between 0.5 and 3.5 μm [49], and high threshold to laser-induced damage. The phase-matching condition is met in type-II configuration, i.e., the high-intensity pump field and the converted telecom photons have perpendicular polarization. Numerical simulations are performed to approximate the required laser power and crystal length for efficient conversion. With this scheme, an internal conversion efficiency as high as 80 % can be reached. With pump laser power up to 400 W available for the experiments, an internal efficiency of approximately 60 % is expected. Since due to the free space interaction no single-mode waveguide coupling (which can result in losses up to 40% [50,51]) is required, the overall device efficiency is expected to reach similar values as in waveguide-based set-ups with larger internal conversion efficiency.

3. DEMONSTRATION OF A LOW-NOISE QFC FOR NV-CENTER EMISSION

3.1. Experimental Set-Up

The experimental set-up is depicted in Fig. 1. The 30 mm-long NLM KTA is placed in a bow-tie cavity (length 46 cm) consisting of three HR-coated mirrors (R_{HR} = 99.95 %) and one coupling mirror (R_{in} = 99 %), in which the incident (coupled) pump power is enhanced by a factor of 40 (60). Two cavity mirrors have a radius of curvature of 100 mm, resulting in a focus diameter of roughly 100 μm inside the NLM.

An amplified fiber laser (NKT ADJUSTIK Y10 and BOOSTIK Y10) provides up to 9 W pump power with a tuning range of 160 GHz. To maintain resonant enhancement at any time, one cavity mirror is mounted to a piezoelectric actuator. A feedback loop implementing the Hänsch–Couillaud locking scheme [52] provides an error signal. Further components are half-wavelength (quarter-wavelength) retardation plates (HWP, QWP) rotating the polarization state of the two input fields and various elements [telescopes, collimation lens (CL), focusing lens (FL)] for efficient coupling of the fields into the cavity and single-mode optical fiber, respectively. To reduce the coupling of any stray light or residual pump light into the optical fiber, the converted light is filtered spectrally by several band-pass and edge-pass filters (BP, optical density of 20 at 1064 nm). The type-II phase-matching condition is met at a crystal orientation of $\Theta \approx 90$ °, $\Phi \approx 30$ ° and a crystal temperature T = 130 °C, where Θ equals the angle between the propagating light and the crystal's z axis, and Φ being the angle between the propagating light and the crystal's x axis measured in the x–y plane. A precise measurement of the angles was not possible due to the limited space between mirrors and crystal.

In this configuration, the phase mismatch of the SPDC process (1064 nm → 1589 nm + 3220 nm) Δk_{SPDC} is of the order of 10^5 m^{-1}, while the gain factor Γ is of the order of 10^1 m^{-1}. The numbers are calculated with the refractive indices of KTA taken from [53]. Therefore, the low-gain approximation of Eq. (3) is valid.

3.2. Results

3.2.1. Conversion Efficiency

The performance of the QFC is quantified by the pump-power dependent rate of telecom photons in the output channel divided by the rate of visible photons in the input channel. This figure is
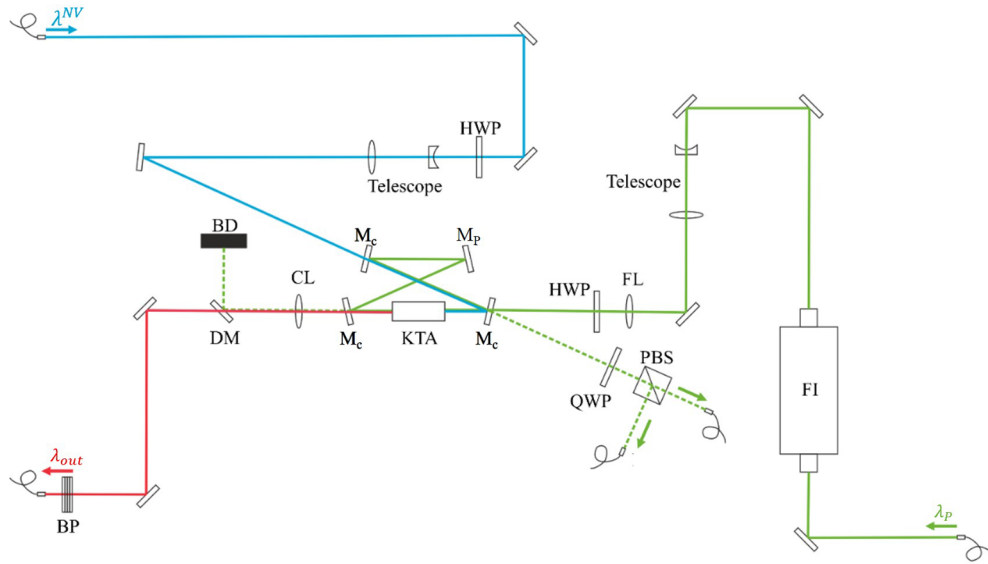
Fig. 1. Schematic drawing of the QFC set-up. The enhancement cavity consists of three mirrors (M_C) and one which is mounted to a piezoelectric actor to control the cavity length (M_P). The nonlinear crystal (KTA) is placed such that the cavity mode's focus is centered inside of it. At the device's signal input/output and pump input, the interacting waves are coupled from free space to fiber or vice versa, indicated by the respective arrow. The solid blue (green, red) lines indicate the beam path of 637 nm (1064 nm, 1589 nm) light, whereas dashed lines denote reflected light and leakages from the cavity, which are either used to implement the cavity control via the Hänsch–Couillaud method or to be filtered from the output field by a dichroic mirror (DM) and further long-pass and bandpass filters (BP). The converted light is coupled to a single-mode fiber behind the BP. Additional components are a Faraday isolator (FI), half-wave plates (HWP), a quarter-wave plate (QWP), focusing and collimation lens (FL, CL), a polarizing beam splitter (PBS), and a beam dump (BD).

called conversion efficiency and takes the following form:

$$\eta_c(P) = \eta_{max} \cdot \sin^2\left(L\sqrt{\alpha_{QFC}P}\right), \tag{5}$$

where η_{max} equals the maximum conversion efficiency including all losses, L is the length of the NLM, and α_{QFC} is the device-specific normalized power efficiency in the low-gain limit [54]. We measure both the internal conversion efficiency, providing general information on the efficiency of the external enhancement cavity approach, and the external conversion efficiency to allow for a comparison to different devices independent of filter set-ups and losses at optical elements. We demonstrate that the internal efficiency can reach similar values compared with waveguide-based QFCs, while the overall losses at optical elements in the device can be significantly smaller. The measurement is conducted with an attenuated cw laser of the same wavelength as the NV-center emission (Toptica DLC DL PRO HP 637, linewidth 300 kHz). The converted power P_{out} is measured behind the dichroic mirror (DM) and behind the single-mode fiber. The pump power in the cavity is calculated by measuring a portion transmitted at one of the cavity mirrors and correcting for the transmission. All error bars and accuracies given in this work are the $1\,\sigma$ interval calculated by combining both statistical deviations and systematic accuracies. The measured ratio of output power to input power is corrected for the wavelength ratio, yielding the photon rate ratio (i.e., conversion efficiency).

The conversion efficiency is measured while sweeping the circulating pump power (see Fig. 2), exhibiting the expected behavior from Eq. (5). A maximum internal conversion efficiency of 60(5) % is measured at a circulating pump power of 360(40) W. Behind the filter stack (transmission $T_{BP} = 90$ %, bandwidth (FWHM) $\Delta\lambda = 3.14(.07)$ nm, center wavelength $\lambda_{BP} = \lambda_{out}$) and after coupling to a single-mode optical fiber (SMF28, coupling efficiency $\eta_{FC} = 80(6)$ %), the external conversion efficiency is

measured to equal 43(5) %. To identify the maximum internal efficiency, the data are fitted to Eq. (5), yielding a maximum value of 80(10) % at a pump power of $\hat{P} = 840(80)$ W and a normalized power efficiency of $\alpha_{QFC} = 3.3(.6)$ W^{-1}m^{-2}. Therefore, a maximum external conversion efficiency of 59(9) % can be extrapolated.

The pump power (peak intensity) is limited to 360 W (9 kW/cm^2) during the experiment by the limited enhancement factor of 60 and imperfect coupling efficiency of pump light to the cavity ($\sim$70 %). With the damage threshold of KTA being of the order of 1 GW/cm^2 [55], it is possible to further optimize the enhancement cavity to enable maximum efficiency.

An investigation of the stability of the circulating pump power while sweeping the pump wavelength with a speed of 20 GHz/min reveals a relative power stability of 10 % (see inset of Fig. 2), which demonstrates the feasibility to maintain a constant output wavelength when the device is operated with photons emitted from NV-center qubits. Note that this tuning speed is determined by the pump laser. It is much larger than required for the typical drift of λ^{NV} (10 MHz/min).

3.2.2. Noise Generation

To determine the rate of noise photons introduced by the QFC, the single-mode optical fiber from the QFC's output is connected to a single-photon detector while pump light is circulating in the cavity and the input beam is blocked. Every detection event recorded can therefore be attributed to either a detector dark count, black-body radiation, stray light, or noise processes in the NLM, e.g., SPDC or Raman scattering of a pump photon. To isolate the pump-induced noise from the constant noise floor resulting from detector dark counts and black-body radiation, measurements are conducted with (without) enabled pump light, while the crystal oven is operating.
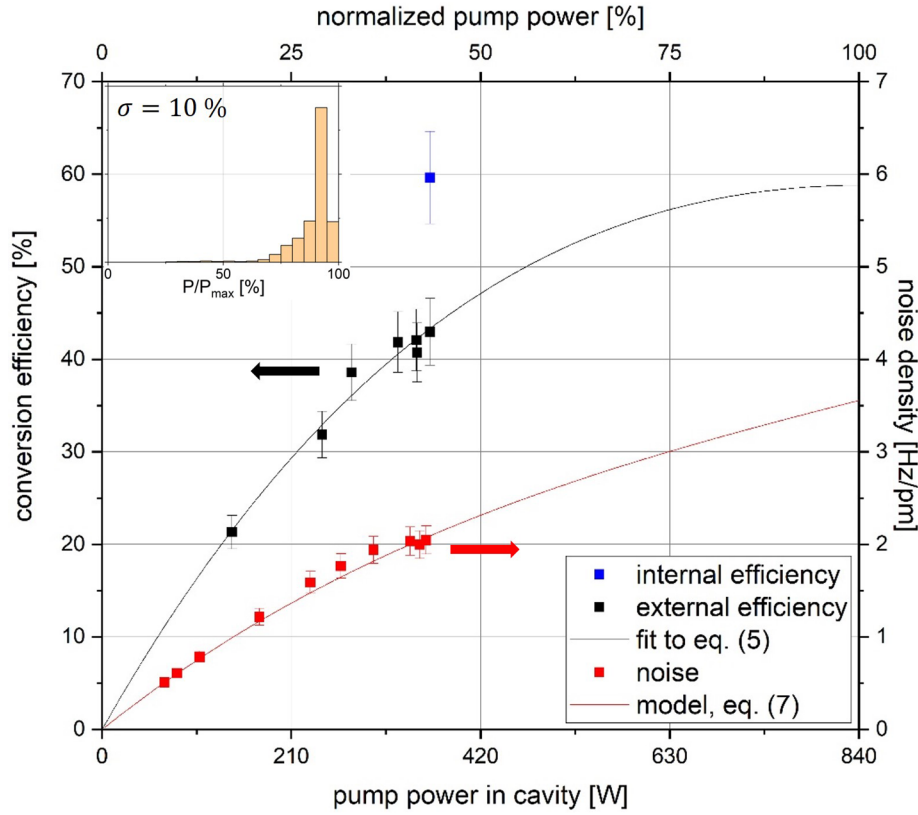
Fig. 2. QFC performance in dependency of the pump power circulating in the enhancement cavity. The absolute pump power is measured with a relative accuracy of 10%, which is omitted for clarity. Conversion efficiency: depicted are both the measurement results for the external and internal efficiency (black and blue squares) and the result of a fit to Eq. (5) (black line). Noise density: depicted are the noise counts normalized to the bandpass' bandwidth (red squares) as well as the model given in Eq. (7) (red line). Inset: Histogram of the circulating pump power normalized to the maximum value P_{max} while tuning the center wavelength by 80 GHz over 4 min.

The noise counts per second N are measured with a superconducting-nanowire single-photon detector (SNSPD, Quantum OPUS One, $\eta_{SNSPD} = 70(5)$ %, dark counts $n_{dc} = 12.4(.2)\,\mathrm{s^{-1}}$). The results are furthermore normalized to the bandwidth of the filter stack, assuming white noise (i.e., $dn/d\lambda = const.$) in this interval:

$$\frac{dn}{d\lambda} = \frac{N}{\eta_{SNSPD} \cdot \Delta\lambda_{BP}}. \qquad (6)$$

In this set-up, an absolute rate of noise events smaller or equal to $4.5 \times 10^3\,\mathrm{s^{-1}}$ is recorded. Correcting for the detector efficiency and normalizing to the filter bandwidth [see Eq. (6)] yields a noise spectral density of the order of single counts per picometer, which is two orders of magnitude smaller than in the former record low-noise QFC set-up for NV-center emission based on a ppLN waveguide at an external (internal) efficiency of 17 % (65 %) [31]. The noise density (averaged over 30 s) while sweeping the pump power is depicted in Fig. 2. The rate of pump-induced noise increases linearly for small pump powers, as it is expected for spontaneous processes [41]. A linear fit to the first three data points yields a non-zero offset of 60 (50) $\mathrm{s^{-1}}$, which is attributed to detector dark counts and black-body radiation originating from the crystal oven which is operated at elevated temperatures. For high pump powers ($> 40\,\% \cdot \hat{P}$), a deviation from this linear dependency is observed. This deviation is attributed to the increasing probability to upconvert a noise photon from λ_{out} to λ_{in} with increasing pump power, effectively

reducing the noise rate at λ_{out}. Following the expression given in [51], we find

$$\frac{dn}{d\lambda} = \frac{1}{\eta_{SNSPD} \cdot \Delta\lambda_{BP}} \cdot \alpha_N P \cdot \left(1 - \frac{\eta_{max}}{2} + \frac{\sin\left(2L\sqrt{\alpha_{QFC}P}\right)}{4L\sqrt{\alpha_{QFC}P}}\right),$$
$$(7)$$

with $\alpha_N = 7.9(.2) \times 10^{-3}\,\mathrm{s^{-1}/pm/W}$ being the internal noise generation coefficient, which equals the slope of the linear approximation at low pump power. The resulting curve (see Fig. 2, red line) well fits the measurement result. To analyze, if Raman scattering or SPDC is the leading noise generation process in this configuration, further measurements must be conducted. The maximum noise density introduced by the QFC equals $2.0(.2)\,\mathrm{s^{-1}/pm}$ ($17(2)\,\mathrm{s^{-1}/GHz}$) at a pump power of $360(40)$ W. At a pump power $\hat{P} = 840(80)$ W with an expected maximum internal efficiency of 80 %, the noise density is extrapolated to $3.6\,\mathrm{s^{-1}/pm}$ ($30\,\mathrm{s^{-1}/GHz}$).

4. CONCLUSION

In this work, we proposed a new approach to frequency down-conversion of single photons from the visible range to telecom wavelengths with a high-intensity pump field at an intermediate wavelength. While periodically poled crystals are used in current-generation quantum frequency converters, resulting in elevated levels of noise photons from spontaneous parametric

downconversion, we investigate a set-up with a birefringently phase-matched conversion scheme in an enhancement cavity resonant for the pump wavelength. The rate of noise photons per wavelength (frequency) interval of 2.0 s^{-1}/pm (17(2) s^{-1}/GHz) generated by scattering processes of the high-intensity pump radiation is smaller by two orders of magnitude compared with ppLN QFCs with waveguided interaction [31] and by a factor of 20 compared with a cavity-assisted ppKTP QFC without a waveguide [36], while the external efficiency of 43 % (at a pump power of 360 W and an internal conversion efficiency of 60 %) is similar. Extrapolations to a pump power of 840 W yield a maximum external conversion efficiency of 59 % with an internal noise photon density of 3.6 s^{-1}/pm (30 s^{-1}/GHz). With the demonstrated enhancement cavity approach, it is possible to reach a conversion efficiency comparable with conventional waveguide-based QFCs due to the mitigated losses by a free space to single-mode waveguide coupling. With an actively controlled enhancement cavity, a tunable pump laser can be used to generate wavelength-tunable telecom photons, which is a crucial prerequisite for the generation of undistinguishable photons from different sources and for active stabilization of the transmission channel. This demonstration paves the way to a new generation of high-performance, low-noise QFCs enabling high-fidelity entanglement generation for future quantum networks.

Disclosures. The authors declare no conflicts of interest.

Data availability. Data underlying the results presented in this paper are not publicly available at this time but may be obtained from the authors upon reasonable request.

REFERENCES

1. H. J. Kimble, "The quantum internet," Nature **453**, 1023–1030 (2008).
2. S. Wehner, D. Elkouss, and R. Hanson, "Quantum internet: a vision for the road ahead," Science **362**, 1 (2018).
3. A. Ekert and R. Renner, "The ultimate physical limits of privacy," Nature **507**, 443–447 (2014).
4. D. Gottesman, T. Jennewein, and S. Croke, "Longer-baseline telescopes using quantum repeaters," Phys. Rev. Lett. **109**, 070503 (2012).
5. L. Jiang, J. M. Taylor, A. S. Sørensen, et al., "Distributed quantum computation based on small quantum registers," Phys. Rev. A **76**, 062323 (2007).
6. S. Ritter, C. Nölleke, C. Hahn, et al., "An elementary quantum network of single atoms in optical cavities," Nature **484**, 195–200 (2012).
7. J. Hofmann, M. Krug, N. Ortegel, et al., "Heralded entanglement between widely separated atoms," Science **337**, 72–75 (2012).
8. L. J. Stephenson, D. P. Nadlinger, B. C. Nichol, et al., "High-rate, high-fidelity entanglement of qubits across an elementary quantum network," Phys. Rev. Lett. **124**, 110501 (2020).
9. D. L. Moehring, P. Maunz, S. Olmschenk, et al., "Entanglement of single-atom quantum bits at a distance," Nature **449**, 68–71 (2007).
10. A. Delteil, Z. Sun, W. Gao, et al., "Generation of heralded entanglement between distant hole spins," Nat. Phys. **12**, 218–223 (2016).
11. R. Stockill, M. J. Stanley, L. Huthmacher, et al., "Phase-tuned entangled state generation between distant spin qubits," Phys. Rev. Lett. **119**, 010503 (2017).
12. H. Bernien, B. Hensen, W. Pfaff, et al., "Heralded entanglement between solid-state qubits separated by three metres," Nature **497**, 86–90 (2013).
13. P. C. Humphreys, N. Kalb, J. P. J. Morits, et al., "Deterministic delivery of remote entanglement on a quantum network," Nature **558**, 268–273 (2018).
14. I. Usmani, C. Clausen, F. Bussières, et al., "Heralded quantum entanglement between two crystals," Nat. Photonics **6**, 234–237 (2012).
15. M. I. G. Puigibert, M. F. Askarani, J. H. Davidson, et al., "Entanglement and nonlocality between disparate solid-state quantum memories mediated by photons," Phys. Rev. Res. **2**, 013039 (2020).
16. D. Lago-Rivera, S. Grandi, J. V. Rakonjac, et al., "Telecom-heralded entanglement between multimode solid-state quantum memories," Nature **594**, 37–40 (2021).
17. R. Riedinger, S. Hong, R. A. Norte, et al., "Non-classical correlations between single photons and phonons from a mechanical oscillator," Nature **530**, 313–316 (2016).
18. C. W. Chou, H. de Riedmatten, D. Felinto, et al., "Measurement-induced entanglement for excitation stored in remote atomic ensembles," Nature **438**, 828–832 (2005).
19. Y. Yu, F. Ma, X.-Y. Luo, et al., "Entanglement of two quantum memories via fibres over dozens of kilometres," Nature **578**, 240–245 (2020).
20. D. Hucul, I. V. Inlek, G. Vittorini, et al., "Modular entanglement of atomic qubits using photons and phonons," Nat. Phys. **11**, 37–42 (2015).
21. V. Krutyanskiy, M. Meraner, J. Schupp, et al., "Light-matter entanglement over 50 km of optical fibre," npj Quantum Inf **5**, 72 (2019).
22. M. Pompili, S. L. N. Hermans, S. Baier, et al., "Realization of a multinode quantum network of remote solid-state qubits," Science **372**, 259–264 (2021).
23. S. Daiss, S. Langenfeld, S. Welte, et al., "A quantum-logic gate between distant quantum-network modules," Science **371**, 614–617 (2021).
24. T. van Leent, M. Bock, F. Fertig, et al., "Entangling single atoms over 33 km telecom fibre," Nature **607**, 69–73 (2022).
25. T. Miya, Y. Terunuma, T. Hosaka, et al., "Ultimate low-loss single-mode fibre at 1.55 μm," Electron. Lett. **15**, 106 (1979).
26. S. Ramelow, A. Fedrizzi, A. Poppe, et al., "Polarization-entanglement-conserving frequency conversion of photons," Phys. Rev. A **85**, 013845 (2012).
27. S. Tanzilli, W. Tittel, M. Halder, et al., "A photonic quantum information interface," Nature **437**, 116–120 (2005).
28. K. de Greve, L. Yu, P. L. McMahon, et al., "Quantum-dot spin-photon entanglement via frequency downconversion to telecom wavelength," Nature **491**, 421–425 (2012).
29. R. Ikuta, Y. Kusaka, T. Kitano, et al., "Wide-band quantum interface for visible-to-telecommunication wavelength conversion," Nat. Commun. **2**, 537 (2011).
30. A. Tchebotareva, S. L. N. Hermans, P. C. Humphreys, et al., "Entanglement between a diamond spin qubit and a photonic time-bin qubit at telecom wavelength," Phys. Rev. Lett. **123**, 063601 (2019).
31. A. Dréau, A. Tchebotareva, A. E. Mahdaoui, et al., "quantum frequency conversion of single photons from a nitrogen-vacancy center in diamond to telecommunication wavelengths," Phys. Rev. Appl. **9**, 064031 (2018).
32. H. Takesue, "Single-photon frequency down-conversion experiment," Phys. Rev. A **82**, 013833 (2010).

33. N. Curtz, R. Thew, C. Simon, *et al.*, "Coherent frequency-down-conversion interface for quantum repeaters," Opt. Express **18**, 22099–22104 (2010).

34. S. Zaske, A. Lenhard, C. A. Keßler, *et al.*, "Visible-to-telecom quantum frequency conversion of light from a single quantum emitter," Phys. Rev. Lett. **109**, 147404 (2012).

35. M. Bock, P. Eich, S. Kucera, *et al.*, "High-fidelity entanglement between a trapped ion and a telecom photon via quantum frequency conversion," Nat. Commun. **9**, 1998 (2018).

36. F. Mann, H. M. Chrzanowski, F. Gewers, *et al.*, "Low-noise quantum frequency conversion in a monolithic cavity with bulk periodically poled potassium titanyl phosphate," Phys. Rev. Appl. **20**, 054010 (2023).

37. P. S. Kuo, J. S. Pelc, O. Slattery, *et al.*, "Reducing noise in single-photon-level frequency conversion," Opt. Lett. **38**, 1310–1312 (2013).

38. J. S. Pelc, L. Ma, C. R. Phillips, *et al.*, "Long-wavelength-pumped upconversion single-photon detector at 1550 nm: performance and noise analysis," Opt. Express **19**, 21445–21456 (2011).

39. J. S. Pelc, C. R. Phillips, D. Chang, *et al.*, "Efficiency pedestal in quasi-phase-matching devices with random duty-cycle errors," Opt. Lett. **36**, 864–866 (2011).

40. C. R. Phillips, J. S. Pelc, and M. M. Fejer, "Parametric processes in quasi-phasematching gratings with random duty cycle errors," J. Opt. Soc. Am. B **30**, 982 (2013).

41. J. S. Pelc, C. Langrock, Q. Zhang, *et al.*, "Influence of domain disorder on parametric noise in quasi-phase-matched quantum frequency converters," Opt. Lett. **35**, 2804–2806 (2010).

42. P. S. Kuo, K. L. Vodopyanov, M. M. Fejer, *et al.*, "Optical parametric generation of a mid-infrared continuum in orientation-patterned GaAs," Opt. Lett. **31**, 71–73 (2006).

43. M. Bass, *Fiber Optics and Nonlinear Optics*, 2nd ed. (McGraw-Hill, 2001).

44. A. Stolk, K. L. van der Enden, M.-C. Roehsner, *et al.*, "Telecom-band quantum interference of frequency-converted photons from remote detuned NV centers," PRX Quantum **3**, 020359 (2022).

45. S. L. N. Hermans, M. Pompili, L. Dos Santos Martins, *et al.*, "Entangling remote qubits using the single-photon protocol: an in-depth theoretical and experimental study," New J. Phys. **25**, 013011 (2023).

46. R. Ikuta, T. Kobayashi, T. Yamazaki, *et al.*, "Cavity-enhanced broadband photonic Rabi oscillation," Phys. Rev. A **103**, 1 (2021).

47. C. E. Vollmer, C. Baune, A. Samblowski, *et al.*, "Quantum up-conversion of squeezed vacuum states from 1550 to 532 nm," Phys. Rev. Lett. **112**, 073602 (2014).

48. E. Arenskötter, T. Bauer, S. Kucera, *et al.*, "Telecom quantum photonic interface for a 40Ca+ single-ion quantum memory," npj Quantum Inf **9**, 34 (2023).

49. G. Hansson, H. Karlsson, S. Wang, *et al.*, "Transmission measurements in KTP and isomorphic compounds," Appl. Opt. **39**, 5058–5069 (2000).

50. B. Albrecht, P. Farrera, X. Fernandez-Gonzalvo, *et al.*, "A waveguide frequency converter connecting rubidium-based quantum memories to the telecom C-band," Nat. Commun. **5**, 3376 (2014).

51. N. Maring, D. Lago-Rivera, A. Lenhard, *et al.*, "Quantum frequency conversion of memory-compatible single photons from 606 nm to the telecom C-band," Optica **5**, 507 (2018).

52. T. W. Hansch and B. Couillaud, "Laser frequency stabilization by polarization spectroscopy of a reflecting reference cavity," Opt. Commun. **35**, 441–444 (1980).

53. K. Kato and N. Umemura, in *Sellmeier and Thermo-Optic Dispersion Formulas for KTiOAsO4. Technical digest (CD)* (Optica Publishing Group, 2004), paper CThT35.

54. R. V. Roussev, C. Langrock, J. R. Kurz, *et al.*, "Periodically poled lithium niobate waveguide sum-frequency generator for efficient single-photon detection at communication wavelengths," Opt. Lett. **29**, 1518–1520 (2004).

55. V. G. Dmitriev, G. G. Gurzadyan, and D. N. Nikogosyan, *Handbook of Nonlinear Optical Crystals* (Springer, 1999).